Electron Tunneling in Proteins: Coupling Through a β Strand

Ralf Langen, I-Jy Chang, Juris P. Germanas, John H. Richards, Jay R. Winkler,* Harry B. Gray*

Electron coupling through a β strand has been investigated by measurement of the intramolecular electron-transfer (ET) rates in ruthenium-modified derivatives of the β barrel blue copper protein *Pseudomonas aeruginosa* azurin. Surface histidines, introduced on the methionine-121 β strand by mutagenesis, were modified with a Ru(2,2′-bipyridine)$_2$(imidazole)$^{2+}$ complex. The Cu^+ to Ru^{3+} rate constants yielded a distance-decay constant of 1.1 per angstrom, a value close to the distance-decay constant of 1.0 per angstrom predicted for electron tunneling through an idealized β strand. Activationless ET rate constants in combination with a tunneling-pathway analysis of the structures of azurin and cytochrome c confirm that there is a generally efficient network for coupling the internal (native) redox center to the surface of both proteins.

Long-range protein ET reactions are key steps in many biological processes (*1*). According to theory (*2*), the rates of these ET reactions are proportional to an electronic coupling factor, $|H_{AB}|^2$, and a Franck-Condon factor (*FC*), which depends on the difference between the reaction driving force ($-\Delta G^0$) and the nuclear reorganization energy (λ). Reactions with $-\Delta G^0 = \lambda$ exhibit maximum rates (k_{max}), which are limited by $|H_{AB}|^2$. The simplest description of H_{AB} treats the medium between donor and acceptor as a one-dimensional square tunneling barrier (1DSB); the rate (k_{ET}) is predicted to drop exponentially as the linear (direct) distance between redox sites (R) becomes greater than the van der Waals contact distance (R_0) (*3*, *4*):

$$k_{ET} = \frac{2\pi}{\hbar} |H_{AB}(R_0)|^2 \exp[-\beta(R - R_0)] (FC) \quad (1)$$

where $\hbar = h/2\pi$ (h is Planck's constant) and β is the distance-decay constant. Dutton and co-workers have demonstrated that a 1DSB model for electron tunneling (Eq. 1), with an exponential distance-decay constant of 1.4 Å^{-1}, provides a rough estimate of coupling strengths for many protein ET systems over a wide range of donor-acceptor separations (*4*).

However, both theoretical and experimental investigations have shown that the structure of the intervening protein medium must be included to provide a semiquantitative description of the tunneling process (*5*–*7*). Beratan and Onuchic and co-workers have developed a tunneling-pathway model to describe electronic couplings between redox sites in a protein (*6*). The protein medium between the two redox sites is decomposed into smaller subunits linked by covalent bonds, hydrogen bonds, or through-space jumps. Each link is assigned a coupling decay, and a structure-searching algorithm is used to identify the optimum coupling pathway between redox sites. This pathway can be described in terms of an effective covalent tunneling length (σ_l), and ET rates should drop exponentially with σ_l rather than with the direct distance between redox sites. A coupling decay of 0.6 per covalent link results in an exponential decay constant of 0.73 Å^{-1} (*8*).

Structure-dependent models of ET predict different coupling efficiencies per unit distance for different secondary structure elements. The individual strands of β sheets define nearly linear coupling pathways along the peptide backbone, whereas in α helices the distance between the termini increases much more slowly (and nonlinearly) with helix length. Hence, at any given donor-acceptor distance, the coupling through a β strand should be greater than that through an α helix. This point is illustrated in Fig. 1, which compares σ_l for an idealized β strand and for an idealized α helix as functions of the terminal β-carbon separation (R_β). The tunneling length for a β strand exhibits an excellent linear correlation with R_β, whereas σ_l for the α helix shows a poorer correlation, especially for $R_\beta \leq 10$ Å. As expected, the best linear fits to the σ_l/R_β plots yield different slopes: 1.72 σ_l/R_β for the α helix and 1.37 σ_l/R_β for the β strand. The near linear σ_l/R_β correlations for the α helix and β strand structures imply that ET rates in these structures should exhibit an exponential dependence on direct distance. The predicted distance-decay constants are 1.26 Å^{-1} for the α helix (*9*) and 1.00 Å^{-1} for the β strand.

We have probed the electronic coupling along a β strand of *Pseudomonas aeruginosa* azurin by attaching Ru(bpy)$_2$(im)$^{2+}$ (bpy, 2,2′-bipyridine; im, imidazole) (*10*) to the surface histidine in each of three site-directed mutants (His^{122}, His^{124}, and His^{126}) of this β barrel blue copper protein (*11*, *12*) (Fig. 2A). Intramolecular ET rates from Cu^+ to Ru(bpy)$_2$(im)(His^X)$^{3+}$ [X = 122, 7.1(4) × 10^6 s^{-1}; X = 124, 2.2(2) × 10^4 s^{-1}; X = 126, 1.3(6) × 10^2 s^{-1}] (numbers in parentheses indicate errors in the last digit) were measured by laser flash transient spectroscopy (Fig. 2B) (*13*). The driving force for these reactions ($-\Delta G^0 = 0.75$ eV) is nearly equal to the estimated reorganization energy for this system (λ ~0.8 eV) (*14*); the observed rates are within 5% of the activationless rates (k_{max}). A plot of log k_{max} versus R_M [R_M, metal-metal separation (*15*)] for Ru-modified azurin is nearly linear (Fig. 2C); the best fit has a distance-decay constant of 1.10 Å^{-1} and a close contact rate (R_M = 3 Å) of 10^{13} s^{-1}. This decay constant is close to the predicted value for coupling along a β strand. The deviation from the β-strand line can be attributed to the fact that the redox sites do not lie on the β-carbon atoms but instead are separated from them by the distances from the β carbons to the metals.

An analysis of the tunneling pathways in azurin requires consideration of the unusual coordination environment of the Cu center. X-ray structure determinations of the azurin active site have shown that the Cu atom has an approximately trigonal bipyramidal coordination (*11*, *16*). The three equatorial ligands are His^{46}, His^{117}, and Cys^{112}. In the axial positions are the carbonyl oxygen of Gly^{45} at 3.0 Å and the

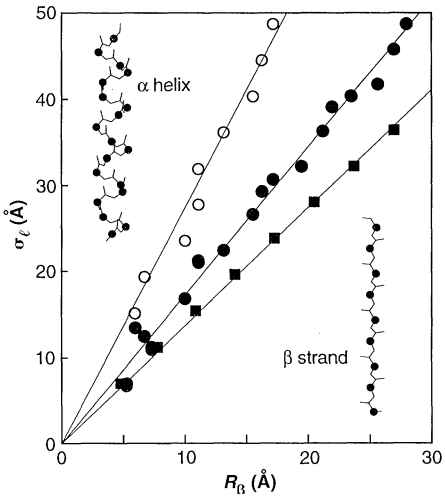

Fig. 1. Plots of tunneling path lengths versus β-carbon separation for idealized peptide secondary structures: α helix neglecting hydrogen-bond interactions (○); α helix including hydrogen-bond interactions (●); and β strand (■). Solid lines are best fits constrained to an intercept at the origin.

Beckman Institute, California Institute of Technology, Pasadena, CA 91125, USA.

* To whom correspondence should be addressed.

sulfur atom of Met[121] at 3.1 Å. These long metal-axial ligand distances complicate calculations of tunneling pathways, because it is not clear whether these interactions should be treated as covalent bonds or as through-space jumps. For the Ru(His^X)-azurin system (X = 122, 124, 126), the coupling involves Met[121]; the close contact rate estimated from a (log k_{max})/σ_l correlation is 10^{13} s^{-1} when the Cu-Met[121] interaction is treated as a space jump (*17*), whereas it is only 10^{12} s^{-1} for a tunneling pathway that includes a covalent Cu–S bond. These values of the close contact rates suggest that the Met[121] sulfur is weakly coupled to the Cu atom, which is in good agreement with the electronic structure calculations of Lowery and Solomon (*18*).

Using the tunneling-pathway model, we compared the results obtained with Ru-modified azurin to those from other Ru-modified proteins with similar donor and acceptor redox potentials. We measured ET rates in eight different Ru(bpy)$_2$(im)(His^X)-modified cytochromes c (cyt c) (*8*, *14*). However, in contrast to the case with Ru-modified azurin, there is no uniform secondary structure type separating the heme and the seven Ru-binding sites (Fig. 3A). Nevertheless, a plot of dominant pathway σ_l versus R_M (Fig. 3B) reveals that a single straight line (slope = 1.45 σ_l/R_M) adequately describes all but two of the Ru binding sites [Ru(His[72])–cyt c and Ru(His[62])–cyt c]. Therefore, log k_{max} should vary linearly with R_M (decay constant = 1.06 Å^{-1}) for all but the His[72] and His[62] data points, an expectation that is largely borne out by the results (Fig. 4). In this analysis, we have used the tunneling-pathway model to identify a family of Ru-binding sites on azurin and cyt c in which the electronic coupling can be described by a single distance-decay constant. In view of the disparate coupling efficiencies of common protein secondary structures (Fig. 1), it is likely that families of binding sites on other (for example, largely α-he-

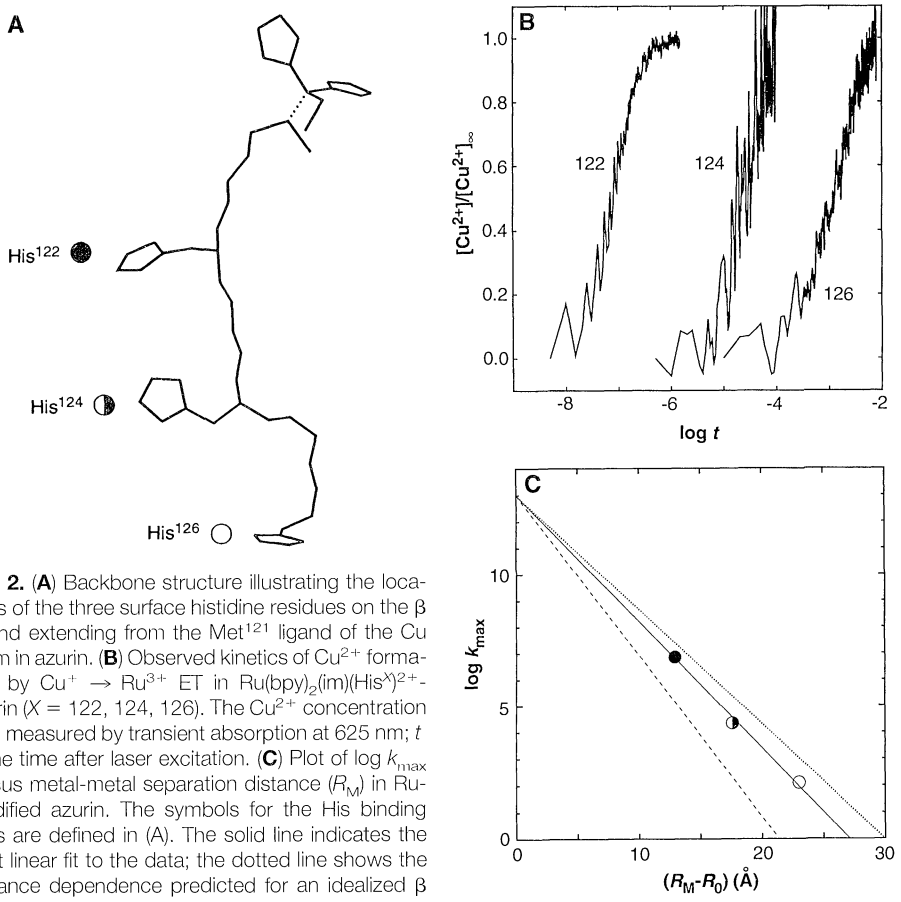

Fig. 2. (**A**) Backbone structure illustrating the locations of the three surface histidine residues on the β strand extending from the Met[121] ligand of the Cu atom in azurin. (**B**) Observed kinetics of Cu^{2+} formation by $Cu^+ \rightarrow Ru^{3+}$ ET in Ru(bpy)$_2$(im)(His^X)$^{2+}$-azurin (X = 122, 124, 126). The Cu^{2+} concentration was measured by transient absorption at 625 nm; t is the time after laser excitation. (**C**) Plot of log k_{max} versus metal-metal separation distance (R_M) in Ru-modified azurin. The symbols for the His binding sites are defined in (A). The solid line indicates the best linear fit to the data; the dotted line shows the distance dependence predicted for an idealized β strand; and the dashed line shows the distance dependence predicted by Dutton and co-workers (*4*). R_0, the close contact distance, is taken to be 3 Å.

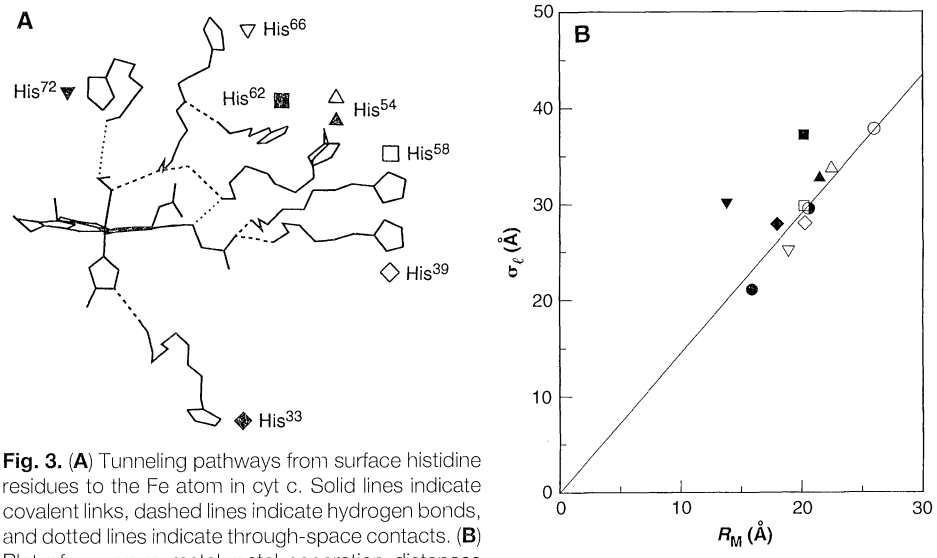

Fig. 3. (**A**) Tunneling pathways from surface histidine residues to the Fe atom in cyt c. Solid lines indicate covalent links, dashed lines indicate hydrogen bonds, and dotted lines indicate through-space contacts. (**B**) Plot of σ_l versus metal-metal separation distances (R_M) in Ru-modified azurin and cyt c. The symbols for the His binding sites of azurin are defined in Fig. 2A and those of cyt c in (A). The solid line is the best linear fit to all but the His[62] and His[72] data points and is constrained to pass through the origin.

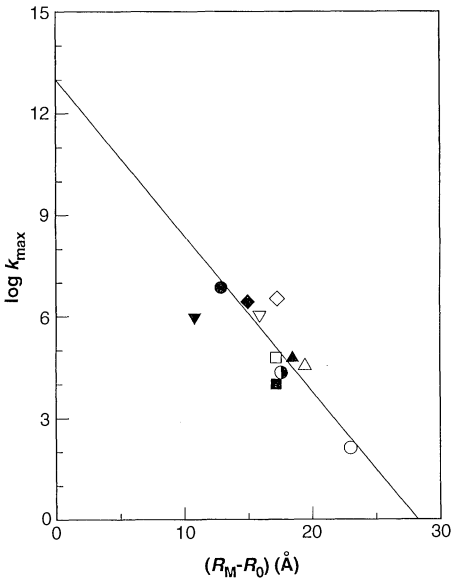

Fig. 4. Plot of log k_{max} versus metal-metal separation distance (R_M) for Ru-modified azurin and cyt c. The solid line is that predicted from the plot of σ_l versus R_M in Fig. 3B; the symbols are the same as those used in Fig. 3.

lical) proteins will exhibit distinctly different distance-decay properties (*19*).

Two key elements determine the distance dependence of electronic coupling in proteins: the directness of the coupling pathway and the energy of the tunneling electron. The former depends on the protein structure and the positions of the redox sites. In the tunneling-pathway model, the tunneling energy defines the covalent-bond coupling decay (ϵ_C); the value of 0.6 derives from analyses of ET rates in model systems (*6*). Changes in ϵ_C will not affect σ_l/R_M correlations, because ϵ_C appears as a prefactor in the expressions for hydrogen-bond and space-gap coupling decays. The magnitude of ϵ_C does, however, determine the predicted slopes in plots of log k_{max} versus distance. The close agreement between the observed and predicted decay constants for azurin and cyt c suggests an ϵ_C value of 0.6 is appropriate for a high-potential oxidant such as $Ru(bpy)_2(im)(His^X)^{3+}$ (potential E^0 = 1.0 V versus the normal hydrogen electrode). In the systems analyzed by Dutton and co-workers (*19*), the redox couples spanned a fairly wide range, but they included many low-potential oxidants. Considering the generally less favorable tunneling energies, the reported protein decay constant [1.4 $Å^{-1}$ (*4*)] accords remarkably closely with the decay [1.26 $Å^{-1}$ (*9*)] predicted for coupling through an α-helical structure.

REFERENCES AND NOTES

1. H. Sigel and A. Sigel, Eds., *Metal Ions in Biological Systems* (Dekker, New York, 1991), vol. 27; I. Bertini, H. B. Gray, S. J. Lippard, J. S. Valentine, Eds., *Bioinorganic Chemistry* (University Science Books, Mill Valley, CA, 1994).
2. R. A. Marcus and N. Sutin, *Biochim. Biophys. Acta* **811**, 265 (1985).
3. J. J. Hopfield, *Proc. Natl. Acad. Sci. U. S. A.* **71**, 3640 (1974); J. Jortner, *J. Chem. Phys.* **64**, 4860 (1976).
4. C. C. Moser, J. M. Keske, K. Warncke, R. S. Farid, P. L. Dutton, *Nature* **355**, 796 (1992); R. S. Farid, C. C. Moser, P. L. Dutton, *Curr. Opin. Struct. Biol.* **3**, 225 (1993).
5. R. A. Friesner, *Structure* **2**, 339 (1994).
6. J. N. Onuchic and D. N. Beratan, *J. Chem. Phys.* **92**, 722 (1990); J. N. Onuchic, P. C. P. Andrade, D. N. Beratan, *ibid.* **95**, 1131 (1991); J. N. Onuchic, D. N. Beratan, J. R. Winkler, H. B. Gray, *Annu. Rev. Biophys. Biomol. Struct.* **21**, 349 (1992); S. S. Skourtis, J. J. Regan, J. N. Onuchic, *J. Phys. Chem.* **98**, 3379 (1994).
7. P. Siddarth and R. A. Marcus, *J. Phys. Chem.* **94**, 8430 (1990); *ibid.*, p. 2985; *ibid.* **96**, 3213 (1992); *ibid.* **97**, 2400 (1993); *ibid.*, p. 13078; A. A. Stuchebrukhov and R. A. Marcus, *ibid.* **99**, 7581 (1995); J. M. Gruschus and A. Kuki, *ibid.* **97**, 5581 (1993); A. Broo and S. Larsson, *ibid.* **95**, 4925 (1991); H. E. M. Christensen, L. S. Conrad, K. V. Mikkelsen, J. Ulstrup, *ibid.* **96**, 4451 (1992); J. W. Evenson and M. Karplus, *Science* **262**, 1247 (1993); O. Farver and I. Pecht, *J. Am. Chem. Soc.* **114**, 5764 (1992).
8. D. R. Casimiro *et al.*, *J. Am. Chem. Soc.*, **115**, 1485 (1993); D. R. Casimiro, J. H. Richards, J. R. Winkler, H. B. Gray, *J. Phys. Chem.* **97**, 13073 (1993); D. S. Wuttke, M. J. Bjerrum, J. R. Winkler, H. B. Gray, *Science* **256**, 1007 (1992).
9. The 1.26 $Å^{-1}$ decay is for hydrogen bond–mediated coupling, which is much more efficient than coupling through the α-helical backbone (2.0 $Å^{-1}$).
10. I-J. Chang, H. B. Gray, J. R. Winkler, *J. Am. Chem. Soc.* **113**, 7056 (1991).
11. E. T. Adman and L. H. Jensen, *Isr. J. Chem.* **21**, 8 (1981).
12. We expressed the proteins in *Escherichia coli* using a T7 polymerase expression system [F. W. Studier, A. H. Rosenberg, J. J. Dunn, J. W. Dubendorf, *Methods in Enzymology* (Academic Press, San Diego, CA, 1990)] and purified by fast protein liquid chromatography (FPLC) according to previously published protocols [T. K. Chang *et al.*, *Proc. Natl. Acad. Sci. U. S. A.* **88**, 1325 (1991)]. The purified proteins were incubated with $Ru(bpy)_2(CO_3)$ and purified again by FPLC. The addition of excess imidazole afforded $Ru(bpy)_2(im)(His^X)$-azurin (*10*).
13. We measured rates of $Cu^+ \rightarrow Ru^{3+}$ ET using a previously described technique (*10*). The $*Ru(bpy)_2(im)(His^X)^{2+}$-$Cu^+$-azurin, generated by means of a 480-nm, 25-ns laser pulse, was oxidatively quenched by 5 mM $Ru(NH_3)_6^{3+}$ to yield $Ru(bpy)_2(im)(His^X)^{3+}$-$Cu^+$-azurin. Subsequent $Cu^+ \rightarrow Ru^{3+}$ ET was monitored by transient absorption at 625, 500, 432, and 310 nm. The slow ET rate in the His^{126} derivative led to a number of complications. With $Ru(NH_3)_6^{3+}$ as a quencher, $Cu^+ \rightarrow Ru^{3+}$ ET was in competition with $Ru(NH_3)_6^{2+} \rightarrow Ru^{3+}$ charge recombination. Consequently, we also measured kinetics using the irreversible quencher $Co(NH_3)_5Cl^{2+}$; consistent results were obtained with the two quenchers. At the protein concentrations used in these experiments (5 to 40 μM), bimolecular $Cu^+ \rightarrow Ru^{3+}$ ET in the His^{126} derivative occurred on the same time scale as intramolecular $Cu^+ \rightarrow Ru^{3+}$ ET; the intramolecular ET rate was extracted from extrapolation of the observed ET rates to infinite dilution.
14. T. B. Karpishin, M. W. Grinstaff, S. Komar-Panicucci, G. McLendon, H. B. Gray, *Structure* **2**, 415 (1994).
15. We obtained all distances by molecular modeling, using the program Enzymix [F. S. Lee, Z. T. Chu, A. Warshel, *J. Comput. Chem.* **14**, 161 (1993)]. We obtained the final distance by averaging the distances in snapshots taken at 1-ps intervals during 200 ps of constrained dynamics simulation. In all cases, convergence was reached after approximately 20 to 30 ps of simulation.
16. G. W. Canters and M. van de Kamp, *Curr. Opin. Struct. Biol.* **2**, 859 (1992); H. Nar, A. Messerschmidt, R. Huber, M. van de Kamp, G. W. Canters, *J. Mol. Biol.* **221**, 765 (1991); *FEBS Lett.* **306**, 119 (1992).
17. The pathway model predicts that the coupling across space gaps drops off as an exponential function of distance (decay constant of 3.4 $Å^{-1}$) (*6*). For the Cu-Met^{121} interaction, the gap is taken as the difference between the observed Cu-S separation and a covalent Cu-S bond distance (~2.3 Å).
18. M. D. Lowery and E. I. Solomon, *Inorg. Chim. Acta* **200**, 233 (1992).
19. Many of the donor-acceptor systems examined by Dutton and co-workers (*4*) are part of the photosynthetic reaction center in which the redox sites are separated by α-helical secondary structures [H. Michel, J. Diesenhofer, J. O. Epp, *EMBO J.* **5**, 2445 (1986)]. Donor-acceptor electronic coupling decays much more rapidly with distance in Ru-modified myoglobin, an α-helical dioxygen-binding protein, than in azurin or cyt c (*8*).

20. We thank D. R. Casimiro, K. Warncke, J. J. Regan, and J. N. Onuchic for helpful comments. Supported by NIH and NSF.

17 January 1995; accepted 23 March 1995

Controlled Folding of Micrometer-Size Structures

Elisabeth Smela,* Olle Inganäs, Ingemar Lundström

Several types of microactuators have been fabricated, from simple paddles to self-assembling and -disassembling cubes. Conducting bilayers made of a layer of polymer and a layer of gold were used as hinges to connect rigid plates to each other and to a silicon substrate. The bending of the hinges was electrically controlled and reversible, allowing precise three-dimensional positioning of the plates. The structures were released from the substrate with a technique based on differential adhesion. This method, which avoids the use of a sacrificial layer and allows the actuators to pull themselves off the surface, may have general applications in micromachining. Possibilities include the manufacture of surfaces whose light reflection or chemical properties can be switched.

As the electronic properties of conjugated, or conducting, polymers are tuned from insulating to metallic, there are concomitant changes in volume: When electrons are donated to or removed from the polymer chains, compensating ionic species are inserted or extracted (*1*). The process can be controlled by the application of a small voltage if the polymer is in contact with an electrolyte. The amount of charge that can be stored is substantial: In fully doped polyheterocyclic polymers, approximately one dopant is incorporated for every four monomer units.

Linköping Institute of Technology, Department of Physics and Measurement Technology, S-581 83 Linköping, Sweden.

*To whom correspondence should be addressed.

Conducting polymers compare favorably with piezoelectric materials, shape memory alloys, and magnetorestrictive materials because they deliver high stresses, have substantial energy densities, and undergo large dimensional changes without requiring high voltages, currents, or temperatures for operation (*2*). Some potential applications of conducting polymers as electromechanical materials have been evaluated conceptually (*3*), and macroscopic bilayer actuators have been demonstrated (*4*, *5*). Recently we produced micrometer-size bilayers (*6*), defining the geometrical elements photolithographically, and conducting polymer-polyimide cantilevers have been made (*7*).

The hinge or artificial muscle component of the devices described here is an